Grand Canonical Monte Carlo study of Argon adsorption in Aluminum nanopores

Francesco Ancilotto, Marco da Re, Sonja Grubisic, Alberto Hernando, Pierluigi Silvestrelli, Flavio Toigo

▶ **To cite this version:**

Francesco Ancilotto, Marco da Re, Sonja Grubisic, Alberto Hernando, Pierluigi Silvestrelli, et al.. Grand Canonical Monte Carlo study of Argon adsorption in Aluminum nanopores. Molecular Physics, 2011, 10.1080/00268976.2011.610369 . hal-00740777

HAL Id: hal-00740777
https://hal.science/hal-00740777

Submitted on 11 Oct 2012

HAL is a multi-disciplinary open access archive for the deposit and dissemination of scientific research documents, whether they are published or not. The documents may come from teaching and research institutions in France or abroad, or from public or private research centers.

L'archive ouverte pluridisciplinaire **HAL**, est destinée au dépôt et à la diffusion de documents scientifiques de niveau recherche, publiés ou non, émanant des établissements d'enseignement et de recherche français ou étrangers, des laboratoires publics ou privés.

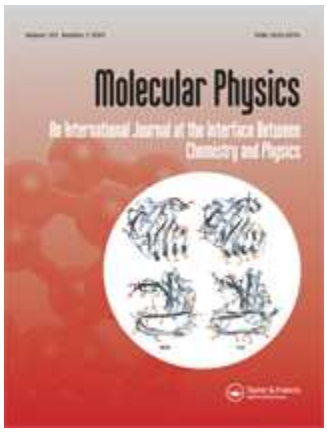

Grand Canonical Monte Carlo study of Argon adsorption in Aluminum nanopores

Journal:	*Molecular Physics*
Manuscript ID:	TMPH-2011-0195.R1
Manuscript Type:	Special Issue in honour of Luciano Reatto
Date Submitted by the Author:	22-Jul-2011
Complete List of Authors:	ancilotto, francesco; University of Padova, Department of Physics Da Re, Marco; University of Padova, Physics Grubisic, Sonja; Institute of Chemistry Technology and Metallurgy Hernando, Alberto; Universitat de Barcelona Silvestrelli, Pierluigi; University of Padova Toigo, Flavio; University of Padova
Keywords:	adsorption, nanopores, fluid
Note: The following files were submitted by the author for peer review, but cannot be converted to PDF. You must view these files (e.g. movies) online.	
paper.tex figures.tar.gz	

SCHOLARONE™
Manuscripts

Molecular Physics
Vol. 00, No. 00, Month 200x, 1–14

INVITED ARTICLE

Grand Canonical Monte Carlo study of Argon adsorption in Aluminum nanopores

F. Ancilotto [a]*, M. Da Re[a], S. Grubišić[b],
A. Hernando[c], P. L. Silvestrelli[a], F. Toigo[a]

[a] *Dipartimento di Fisica 'G. Galilei', Università di Padova, via Marzolo 8, I-35131 Padova, Italy and CNR-IOM-Democritos, I-34014 Trieste, Italy* ; [b] *Institute of Chemistry Technology and Metallurgy, Njegoseva 12, 11001 Belgrade, Serbia* [c] *Departament ECM, Facultat de Física, and IN²UB, Universitat de Barcelona. Diagonal 647, 08028 Barcelona, Spain*

(*Received 00 Month 200x; final version received 00 Month 200x*)

We present a theoretical study of Argon adsorption on a model Aluminum substrates structured with cylindrical nanopores. We employ state-of-the-art computational methods to obtain i) accurate three-dimensional adsorption potentials for the nanostructured substrate starting from the corresponding *ab initio* physisorption potential for a planar surface, and ii) the adsorption and desorption isotherms by means of Grand Canonical Monte Carlo simulations. We study the effect of pore shapes upon Argon adsorption in the case of a substrate characterized by a periodic arrangement of identical cylindrical nano-pores, open at both ends or with one end closed. We find the occurrence of hysteresis loops between adsorption and desorption cycles in open-end pores, in accordance to recent experiments and to previous theoretical approaches. At variance with the prediction of the empirical Cohan's law, we also find hysteresis in pores with one closed end.

1. Introduction

Over the last decade, the rapid development of nanotechnologies, especially synthesis and modification of novel nanostructured materials, has raised the attention of theoreticians and experimentalists to the properties of fluids confined in nanostructured materials. In particular, nanoporous materials possess a unique set of properties, absent in the bulk materials such as high specific areas, fluid permeability, molecular sieving and shape-selective properties. Different nanoporous materials with varying pore size, porosity, pore size distribution and composition have different adsorption properties that will eventually determine their potential applications. For instance, pores with open ends are often required for catalysis, filtration or membranes, while pores with one closed end are useful in sonic and thermal insulation, or lightweight structural applications.

The adsorption/desorption process of fluids in mesoporous materials often exhibits hysteretic behavior. This phenomenon is usually associated with the occurrence of capillary condensation and evaporation transitions. In 1932, Foster [1] advanced a classical argument, claiming that hysteresis is an intrinsic property of the phase transition in a single idealized pore. In particular, hysteresis could be associated with the appearance of a very large number of metastable states,

*Corresponding author. Email: franc@pd.infn.it

ISSN: 0040-5167 print/ISSN 1754-2278 online
© 200x Taylor & Francis
DOI: 10.1080/0040516YYxxxxxxxx
http://www.informaworld.com

For Peer Review Only

which are local minima of the free energy (or the grand potential) corresponding to different configurations of the fluid density [2, 3].

In general, during the adsorption cycle in an idealized infinite cylindrical pore, the adsorbate is located on the pore walls. Capillary filling takes place at a vapor pressure which is lower than the thermodynamic vapor–liquid coexistence pressure of the bulk phases. From a microscopic point of view, this process follows from density fluctuations in the gaseous region, which must produce large enough liquid droplets to act as condensation nuclei. The pore ends (if both open) do not alter the mechanism which gives rise to condensation, but they change dramatically the evaporation (emptying) mechanism, which starts instead from a hemispherical meniscus at each end of the pore, which progressively recedes [4].

The equilibrium vapor pressure P for a liquid-vapor interface with mean curvature H is given by the classical Kelvin's equation:

$$ln\left(\frac{P}{P_{sat}}\right) = -2H\frac{\gamma V_L}{RT} \tag{1}$$

where P_{sat} is the saturated vapor pressure, γ is the liquid–gas surface tension at temperature T, V_L is the molar liquid volume and R is the ideal gas constant. A generalization of the Kelvin equation for capillary condensation including the interaction with the substrate is contained in Ref.[5].

Cohan' argument [6] allows to understand adsorption hysteresis within cylindrical pores. During the condensation on the pore walls, the meniscus has a cylindrical shape and its mean curvature H is $[2(r-t)]^{-1}$, where r is the pore radius and t the thickness of the adsorbate. The mean curvature of each of the two hemisperical evaporation meniscii is instead $(r-t)^{-1}$; this yields a numerical factor 2 in the Kelvin equation between the two cases, thus explaining the hysteresis. The irreversibility of the adsorption process in a cylindrical or slit-like pore with open ends has been predicted by a variety of molecular modeling methods [4, 7–12].

The situation is different, in principle, in pores with one closed end: there, hysteresis should not be observed because during both adsorption and desorption cycles the meniscus is hemispherical, so the isotherms for each branch should be identical. A large number of experimental works, however, show that hysteresis is sometimes present in adsorption within closed-end pores. For example, experimental investigations of adsorption of nitrogen [13] or argon [14] on mesoporous silicon show pronounced hysteresis loops, irrespective of whether the pores are open at one or at both ends.

Capillary condensation is governed by the strength ratio and range of the fluid-fluid and the fluid-substrate interaction [15], therefore the disorder of the pore walls associated with local differences in the pore diameter and/or with the presence of defects/impurities should affect in a measurable way the adsorption within pores. For this reason, when hysteresis is present in adsorption within closed-end pores, it is usually attributed to disorder which, in the first place, is sourced from size differences among the pores of a matrix. Sometimes, analysis of the hysteresis loop is carried out just in order to estimate the pore size distribution [16]. The assumption of disorder as reason behind hysteresis has been confirmed by the results of theoretical works, such as in [17] where adsorption on a silica xerogel and on a porous glass (examples of a disordered material) are simulated. Surface roughness and morphological defects, such as constrictions, were simulated [18–21] as well; and the inkbottle geometry [10, 21, 22] has been often taken as prototype for the local differences in the pore diameter. Puibasset *et al.* [23, 24] studied the effect of topological and chemical heterogeneities of the pore walls, through suitable modu-

For Peer Review Only

lations of the external potential; moreover, it has been shown that any modulation of the fluid/wall interaction strongly affects the adsorption isotherms [23, 25].

A thermodynamic approach to the effect of pore space connectivity was provided in Ref.[26]; even when pores are physically separated, when they are completely filled, they are connected by the liquid film on the planar external surface, so network effects can arise anyway [27, 28]. The liquid film might prevent the concave meniscus from passing through each pore at the expected equilibrium pressure (as predicted, e.g., by Kelvin's equation), the emptying of the pore being due by the tearing of the film at the edges of the pore, as proposed in Ref.[13]. The hysteresis may depend upon the temperature, pore diameter, shape of meniscus or surface heterogeneity of the pore walls, so that the absence of hysteresis beyond a certain diameter or temperature could be observed in some cases[29].

The elastic deformations of the porous material during the gas adsorption may also be related to the presence of hysteretic behavior [30–32]. It was found that the pores interact through the elastic deformation of their walls whether they are interconnected or not [31]. Although the adsorption of gases inside cylindrical pores with one closed end has been studied in a few theoretical papers [4, 7, 8, 10, 11, 24], the behavior of condensable vapors in this kind of pores, and in particular the very nature (irreversible vs. reversible) of the adsorption process, is still a debated issue.

The main motivation of this work is to apply state-of-the-art computational tools to study the entire adsorption/desorption cycle of Ar on a nanoporous substrate. For the choice of the substrate we were inspired by the experiments on Ar adsorption within alumina substrates characterized by a controlled presence of an ordered array of pores described in Ref. [16, 33], which reveal hysteresis loops between adsorption and desorption cycles, even in the case of pores closed at one end. A low degree of disorder is suggested by the shape of the loops: H1-type (quasi parallel adsorption and desorption branches), instead of the usual H2-type (asymmetric loop, with a desorption branch much steeper than the adsorption branch) [34]. Following this experimental setup, we have simulated the adsorption of an Ar fluid on a chemically simpler aluminum substrate, structured with a regular arrangement of cylindrical nanopores, either open at both ends or with one closed end. To this aim: (i) we have applied the elementary source method, described in Sec.2.2, to obtain, starting from an accurate *ab initio* physisorption potential for the planar Al surface, a full three-dimensional potential for these nanostructured substrates, and (ii) we have computed the Argon adsorption isotherms on such substrates, at $T = 85$ K, by means of Grand Canonical Monte Carlo simulations (see Sec.2.1).

At variance with the predictions of Cohan's model, we find clear hysteretic behavior for closed end pores. We believe this is due to a so far overlooked effect, i. e. the formation of a planar film around the pore mouth. During desorption, a energy barrier for ripping such film gives rise to hysteresis. We will discuss experimental evidence for such effect in Sec.3.

2. Computational methods

We briefly describe, in this Section, our implementation of the Monte Carlo algorithm, by means of which the calculations have been performed, and the way to calculate the external potential, namely the elementary source method [35], starting with an accurate interaction potential between an Ar adatom and an Al planar surface.

The Ar–Ar interaction is described by the bare Lennard–Jones potential, with $\epsilon = 119.8$ K and $\sigma = 3.41$ $\mathring{A}$; this is known to reproduce quite accurately the coexistence curve of Argon both in the gas and the liquid phase below the critical

For Peer Review Only

point [36].

2.1. *Grand Canonical Monte Carlo method*

The Monte Carlo simulations were carried out in the Grand Canonical ensemble. This has the main advantage of accounting for density fluctuations at fixed temperature T and chemical potential μ, which allows us to properly study interfacial phenomena where two phases (vapor and liquid), which can exchange particles, are at equilibrium in the presence of an external substrate potential. This is possible by the random insertion and deletion of atoms [37]: the move is accepted according to the usual Metropolis formula [38], i. e. with probability:

$$P\left(N \rightleftharpoons N+1\right) = \max\left\{1, \left[\frac{V\Lambda^{-3}}{N+1}\, e^{\mu/k_BT} e^{-(E_{N+1}-E_N)/k_BT}\right]^{\pm 1}\right\} \tag{2}$$

whereas the probability for the displacement of a single particle is:

$$P\left(N \rightarrow N\right) = \max\left\{1, e^{\Delta E/k_BT}\right\} \tag{3}$$

where Λ is the thermal de Broglie wavelength, k_B the Boltzmann constant, and E_N (E_{N+1}) the internal energy of the configuration with N ($N+1$) atoms: it includes the contribution of the thermalized kinetic energy, the interparticle interaction and the interaction with the substrate.

The fraction of trials for atom displacement, insertion, and removal amounted to 50%, 25% and 25% respectively; the maximum allowed displacement was adjusted in order that the displacement acceptance ratio were 50%. Once the equilibrium is reached, the system is sampled at regular intervals. We have chosen the number of moves in order to sample the system every $5 \div 10$ times the number of atoms, and to collect $6000 \div 10000$ samples altogether: with this choice, consecutive samples are essentially uncorrelated.

In studying adsorption, we begin with a large, negative value for the chemical potential μ and very few atoms in the cell. When studying desorption, we initialize the system with the final configuration of the adsorption branch with the highest chemical potential. In both adsorption and desorption cycles, each simulation at a given μ is always started from the equilibrium atomic configuration obtained with the previous value of μ.

2.2. *The substrate adsorption potential*

In a recent work [39], Silvestrelli *et al.* have obtained the physisorption potential of an Argon atom on the Al(100) surface by means of *ab initio*-DFT calculations, modified to include Van der Waals (VdW) interactions. In particular, the binding energies and equilibrium distances on different surface adsorption sites have been computed, together with the dependence of the average adsorption potential on the adatom–surface distance z.

We derive here, from the results reported in Ref. [39], an effective potential which represents the overall adsorption properties of a planar model Al surface. In particular, we average the calculated potentials over the different adsorption sites, for a given distance from the surface, in order to obtain a function depending only

For Peer Review Only

on z. The resulting potential has a minimum value $V_0 = -72.27$ meV at a distance $z_0 = 4.66$ Å. Although the inclusion of VdW effects is expected to give reliable values for the binding energy and equilibrium distance of the Ar atom, a proper calculation of the long-range tail of the adatom–surface potential (which behaves as $-C_3/z^3$,) using the *ab initio* approach of Ref. [39] is difficult, due to the very big size required for the supercell. For this reason, we use for C_3 the value computed by direct summation of the frequency-dependent polarizabilities [40]. The potential $V_s(z)$ describing the interaction between an Ar atom and an Al planar surface has been obtained by fitting the *ab initio* results to a simple functional form, written in terms of a short-range repulsion and long-range van der Waals attractions:

$$V_s(z) = \frac{A}{z^9} - \frac{C_5}{z^5} - \frac{C_3}{z^3} \tag{4}$$

The two free parameters A and C_5 are adjusted in such a way to reproduce both the minimum depth V_0 and position z_0 in the potential as computed in our *ab initio* calculations. Proceeding this way, we obtained: $A = 8.25497 \times 10^4$ eV Å^9, $C_3 = 1.490$ eV Å^3 and $C_5 = 2.95683 \times 10^2$ eV Å^5.

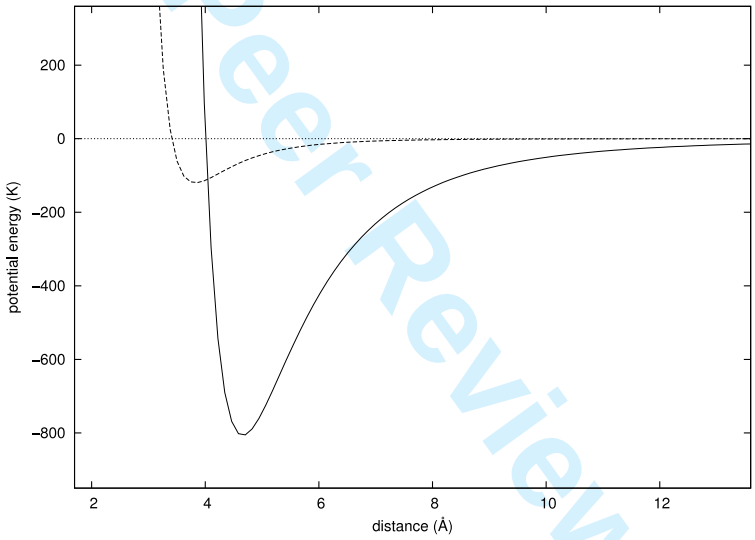

Figure 1. Comparison between the Ar–Ar potential (dashed line) and the average Ar–Al surface potential (solid line).

The Ar–Al surface average potential is plotted in Fig. 1, as a function of the Ar surface distance. For comparison, the much weaker Ar–Ar interatomic potential is also shown.

To accurately describe the interaction of Ar atoms with a much more complex substrate characterized by the presence of nanopores, we adopt here the elementary source method [35], which allows us to determine the adsorption potential for arbitrary geometries, provided the adsorption potential for the planar surface is known. Assuming a continuous distribution of matter, this technique derives the elementary contribution of a differential source, which can afterwards be integrated, weighted with a density that corresponds to an arbitrary surface topology, like cavities, wedges, pores, etc., to produce the adsorption potential for a foreign atom interacting with such a substrate. The method is numerically fast and robust, and gives rise to potential landscapes properly accounting for the topology of the

For Peer Review Only

surface. If the solid is defined by the inequality $\psi(\mathbf{r}) > 0$, the potential energy $V_{ext}(\mathbf{r})$ for an atom at $\mathbf{r}$ is computed as:

$$V_{ext}(\mathbf{r}) = \int \frac{d\mathbf{r}'}{2\pi} H\left(\psi\left(\mathbf{r}'\right)\right) \frac{V_s''\left(|\mathbf{r}-\mathbf{r}'|\right)}{|\mathbf{r}-\mathbf{r}'|} \tag{5}$$

where H is the Heaviside function and V_s is the interaction potential between the adatom and the planar surface made of the same material. In our case, although $V_{ext}(\mathbf{r})$ has been computed only inside the supercell, in order to accurately reproduce the effect of the periodic arrangement of pores, the first neighboring cells have been included in the integration.

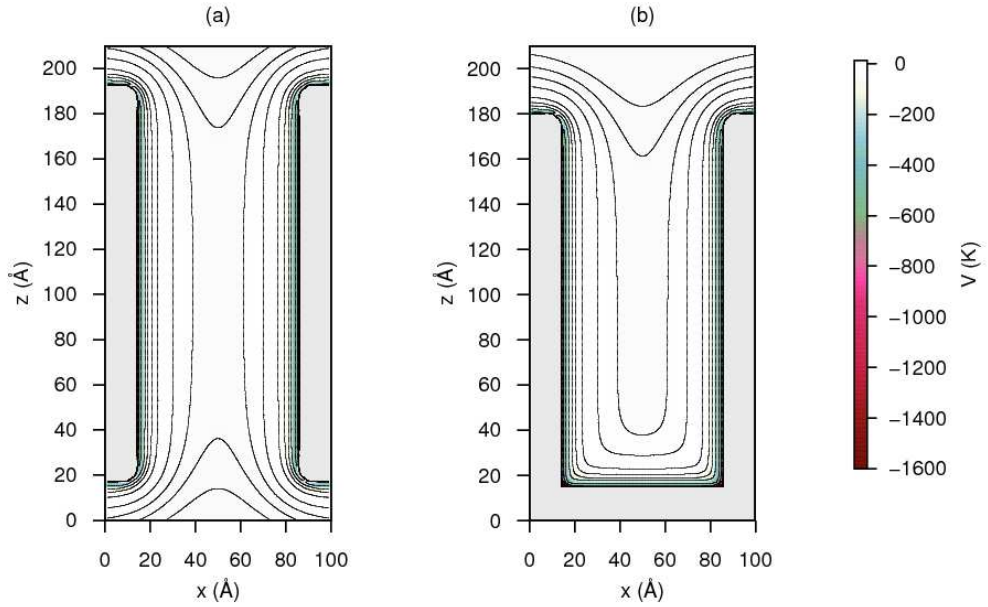

Figure 2. Maps of the interaction potential between an Ar atom and an Al pore (a) open at both ends and (b) closed at one end. The isopotential lines correspond to: -0.01, -0.5, -1, -2, -5, -10, -20, -50, -100, -200, -500, -800, -1000, -1200, -1400 K.

3. Results and discussion

Two models of nanopores have been considered in the present work: cylindrical pores open at both ends and cylindrical pores closed at one end. Their diameter is $D = 70\ \mathring{A}$ and their length is $L = 165\ \mathring{A}$. The supercell sizes are: $L_x = L_y = 100\,\mathring{A}$ and $L_z = 210\,\mathring{A}$, z being the direction of the pore axis. We have considered one pore per supercell: due to our use of periodic boundary conditions, as described in Sec.2, this actually results in a regular arrangement (square lattice) of identical parallel pores on an Al thin slab, each pore axis being 100 $\mathring{A}$ distant from its first neighbor pores. This is the situation encountered in experiments [33], i. e. substrates patterned with regular arrays of nanopores rather than single, isolated pores.

For Review Only

A vacuum region about 30 $\mathring{A}$ thick is added in order to decouple the repeated images of the slab along the z-axis, and to allow for the formation of a sufficiently thick vapor buffer in equilibrium with the adsorbed liquid. In the case of closed pores, at the top of the supercell a purely repulsive potential wall is added to the pore potential to keep the atoms inside the supercell during the simulations.

The landscapes of the Ar-substrate potentials associated with such geometries, computed as described in the previous Section, are shown in Fig. 2.

We have computed, using the GCMC method described in the previous Section, the Ar isotherms at $T = 85$ K, for both adsorption and desorption. Isotherms are defined as relations between the coverage $\Gamma = \frac{1}{S}\int d\mathbf{r}\left(\rho\left[\mathbf{r}\right) - \rho_v\left(\mathbf{r}\right)\right]$ and the chemical potential μ. Due to the very low vapor density at the studied temperature ($T = 85\,\mathrm{K}$), Γ practically coincides, up to a scale factor, with the total number of atoms N in the supercell. The experimental counterpart of the coverage thus defined is the amount of fluid adsorbed on the substrate in torsional microbalance experiments, like the ones described in Ref. [16].

The chemical potential μ is related to the vapor pressure p by [41] :

$$\frac{\mu - \mu_{id}}{k_B T} = -\ln\left(1+Q\right) + 2Q \tag{6}$$

where $Q = \left(\left(4Bp/T+1\right)^{1/2} - 1\right)/2$, μ_{id} is the chemical potential of the ideal gas and B is the second virial coefficient of Ar.

The adsorption and desorption cycles are simulated by systematically increasing or decreasing the chemical potential, using the final, equilibrium configuration for a given μ as the initial configuration for the next value of μ.

We first computed the isotherm for Ar adsorption on the planar Al surface described by the adsorption potential Eq. (4). Since no hysteresis loop is possible in such translationally-invariant geometry, the isotherms are the same along the adsorption and desorption paths. We show in Fig. 4 our results at T=85 K: Plateaus are present at low coverages, which are due to the layer-by-layer growth of the adsorbed fluid, each plateau being associated with the successive completion of single Ar atomic layer. A few density profiles corresponding to the early stages of adsorption on the planar surface are shown in Fig. 3

We verified that, closer to the coexistence value of μ (rightmost part of Fig. 4), the coverage dependence upon $\Delta\mu \equiv \mu - \mu_{coex}$ follows the Frenkel-Halsey-Hill power law $N \propto (\Delta\mu)^{-1/3}$ expected for the growth of a planar film under the action of non-retarded Van der Waals interactions.

Next, we performed GCMC simulations of the adsorption/desorption process of Ar, at $T = 85$ K, inside the periodic arrangement of cylindrical nanopores, both open-ended and closed-ended, described previously.

We show in Fig. 5 the computed isotherm for the open-ended pore (a) and for the closed-ended pore (b). According to the IUPAC classification [34], both the isotherms correspond to a type IV (typical of monolayer/multilayer adsorption in mesopores) and the hysteretic behavior to a type H1 (parallel adsorption and desorption branches). Both type of pores show hysteresis loops in the isotherms, whereas from Cohan's argument the closed pores should not exhibit hysteresis. We will discuss in the following a possible reason for such apparently anomalous behavior.

We show in Fig. 6) selected atomic equilibrium configurations at different chemical potentials, illustrating the adsorption/desorption processes in the open-ended pore arrangement. The adsorption process within the pore starts with the for-

For Peer Review Only

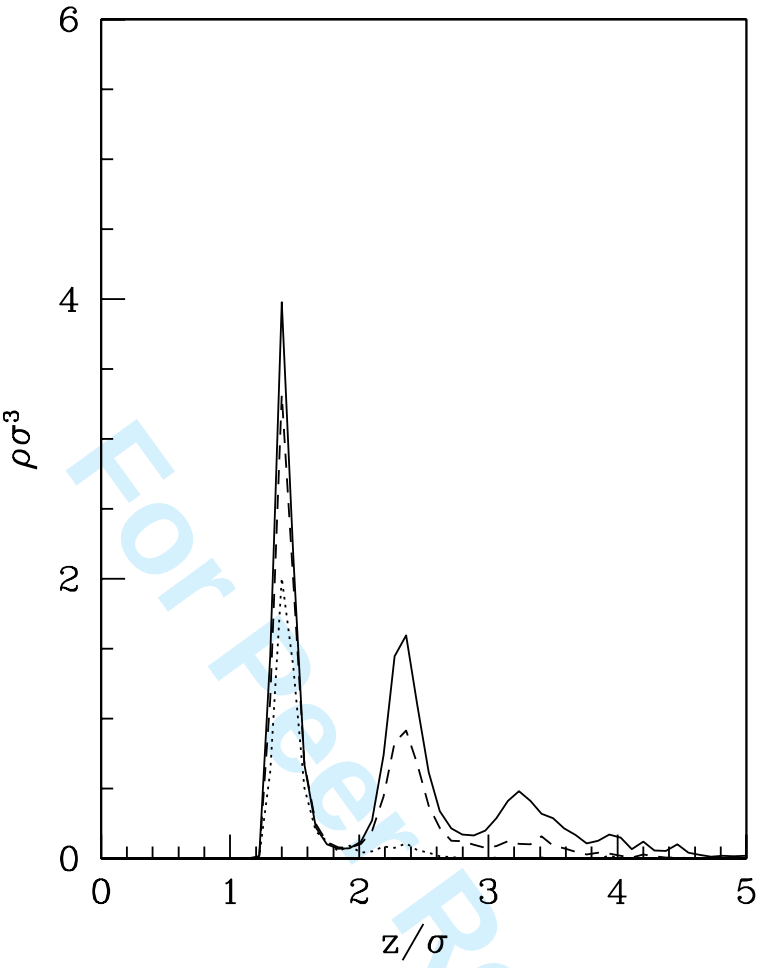

Figure 3. Density profiles corresponding to the early stages of Ar adsorption on a planar Al surface. Displayed quantities are in units of the Ar-Ar Lennard-Jones parameter $\sigma = 3.41\,\mathring{A}$ (see text).

mation of a monolayer on its inner wall. The associated density has a maximum value which is higher than the bulk density, and it is located at the Al surface - Ar potential energy minima. As the chemical potential increases, growth proceeds initially in a layer-by-layer manner. At higher coverages, the density along the pore axis becomes appreciable, leading to capillary filling of most of the pore region (although with a lower density along the pore axis) ($\Delta\mu \cong$ -31.4 K, Fig. 6a). At this point the meniscus shape changes from cylindrical to hemispherical, while the two newly created meniscii move towards the pore mouths as the chemical potential is further increased. The pore filling is accompanied by a steep increase in coverage with μ, which is followed, once the pore is almost completely filled, by a much less steep increase of the coverage with μ (starting from $\Delta\mu \cong$ -29.0 K, Fig. 6b). This latter regime corresponds to configurations where the two meniscii, pinned at the pore mouths, gradually decreases their curvature (Fig. 6c). Eventually, the curved meniscii merge with the thin film already present on the flat portion of the surface around the pore entrances, and the isotherm slope increases again, leading to the usual Frenkel-Halsey-Hill law $N \propto \Delta\mu^{-1/3}$, as expected for a flat surface. We can only see the early stages of such regime, because of the finite size of our supercell along the z-direction.

For Peer Review Only

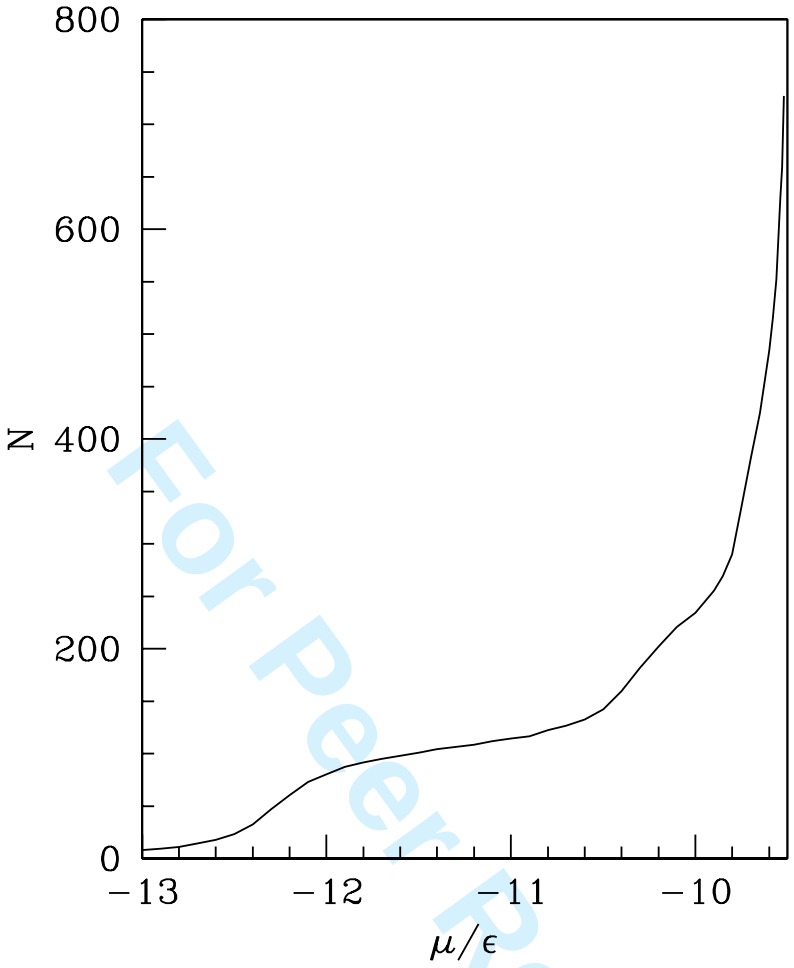

Figure 4. Calculated isotherm (at T=85 K) for the planar Al surface. The chemical potential is expressed in units of the Ar-Ar Lennard-Jones parameter $\epsilon = 119\,K$.

The desorption cycle proceeds through the development of two hemispherical meniscii at each of the pore ends. As the chemical potential decreases, first the meniscii increase their curvature but remain pinned to the pore mouths, then they recede until the two fluid surfaces start interacting and ($\Delta\mu \cong$ -59.3 K, Fig. 6d) the system eventually jumps to a more stable low-coverage configuration where the fluid mainly wets the pore inner wall.

From the density configurations shown in Fig. 6, it appears that, in addition to the localization perpendicular to the surface of the pore which gives rise to a marked layer structure, additional localization within each monolayer occurs along the monolayer plane (see in particular Fig. 6b) suggesting a partially solid-like nature of the adsorbed Ar in the pore interior.

In the case of a closed pore, in the early stages of adsorption (i.e. very negative μ values), a solid-like monolayer film covers the lateral and the bottom inner surface of the pore; the region at the bottom of the pore, along its contour, is covered first because of the stronger attraction, and the adsorbate density there is higher. Once the bottom of the pore is covered, a roughly hemispherical meniscus eventually forms (see Fig. 7b). As more atoms are adsorbed, the meniscus moves towards the pore entrance, until the whole pore is filled with Argon. The computed isotherms

For Peer Review Only

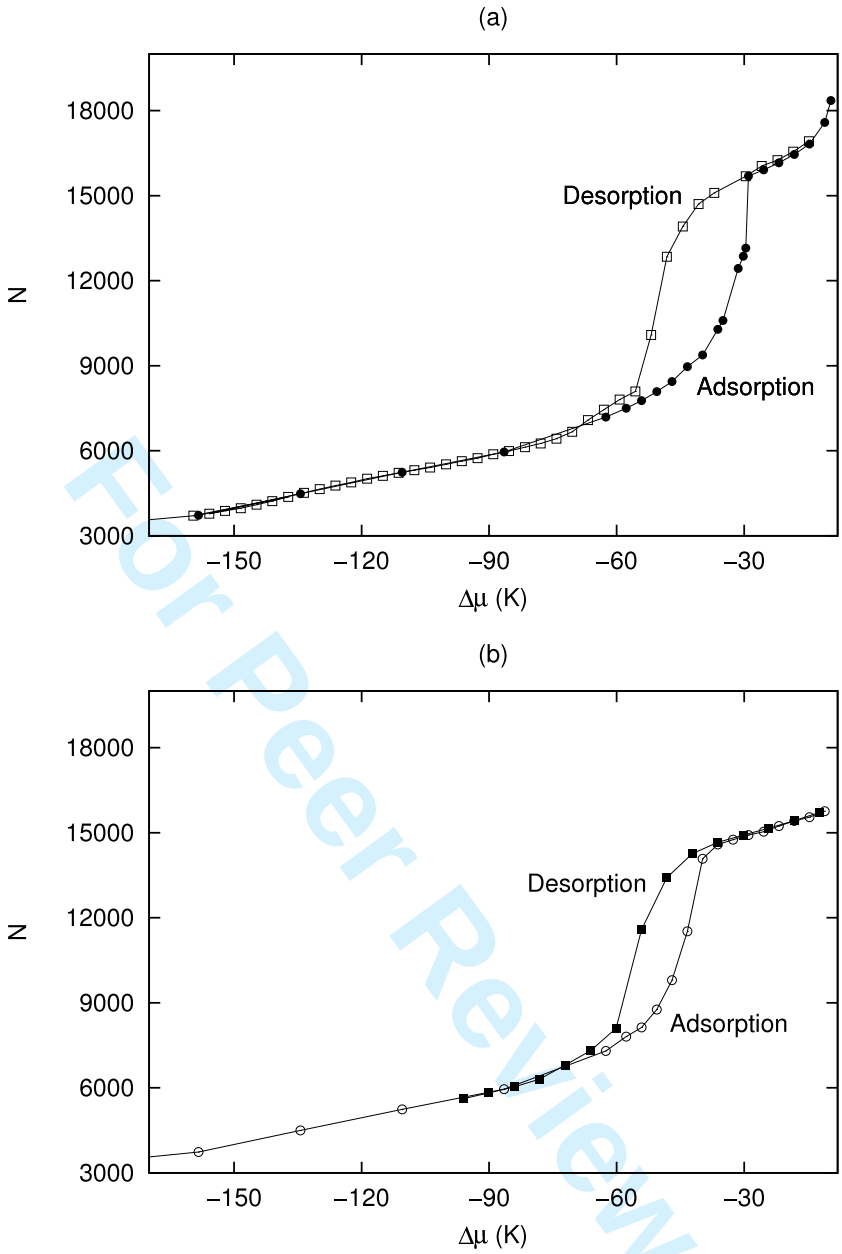

Figure 5. (a) adsorption (bullet) and desorption (squares) isotherms ($T = 85$ K) of Ar in pores open at both ends; (b) adsorption (○) and desorption (black squares) isotherms ($T = 85$ K) of Ar in pores closed at one end.

are shown in Fig. 5b. We notice that there is an hysteresis loop also in the case of adsorption within closed-ended pores, although it is narrower than that for the open-end pores.

The desorption branch of the hysteresis loop for closed-ended pores occurs roughly at the same μ values as for open-ended pores, as expected since in both cases desorption proceeds with hemispherical meniscii.

The adsorption branch of such loop is instead located at lower values of μ than in the case of open-end pores. The difference $\Delta\mu$ between these two values is $\Delta\mu \sim 15K$, and it is roughly accounted for by the differences in the curvature between the hemispherical meniscus in the closed-end pore and the cylindrical meniscus in the open pore. We have computed, using Eq. (1) and Eq. (6), the expected difference in chemical potential due to a cylindrical and hemispherical meniscus, and found

For Peer Review Only

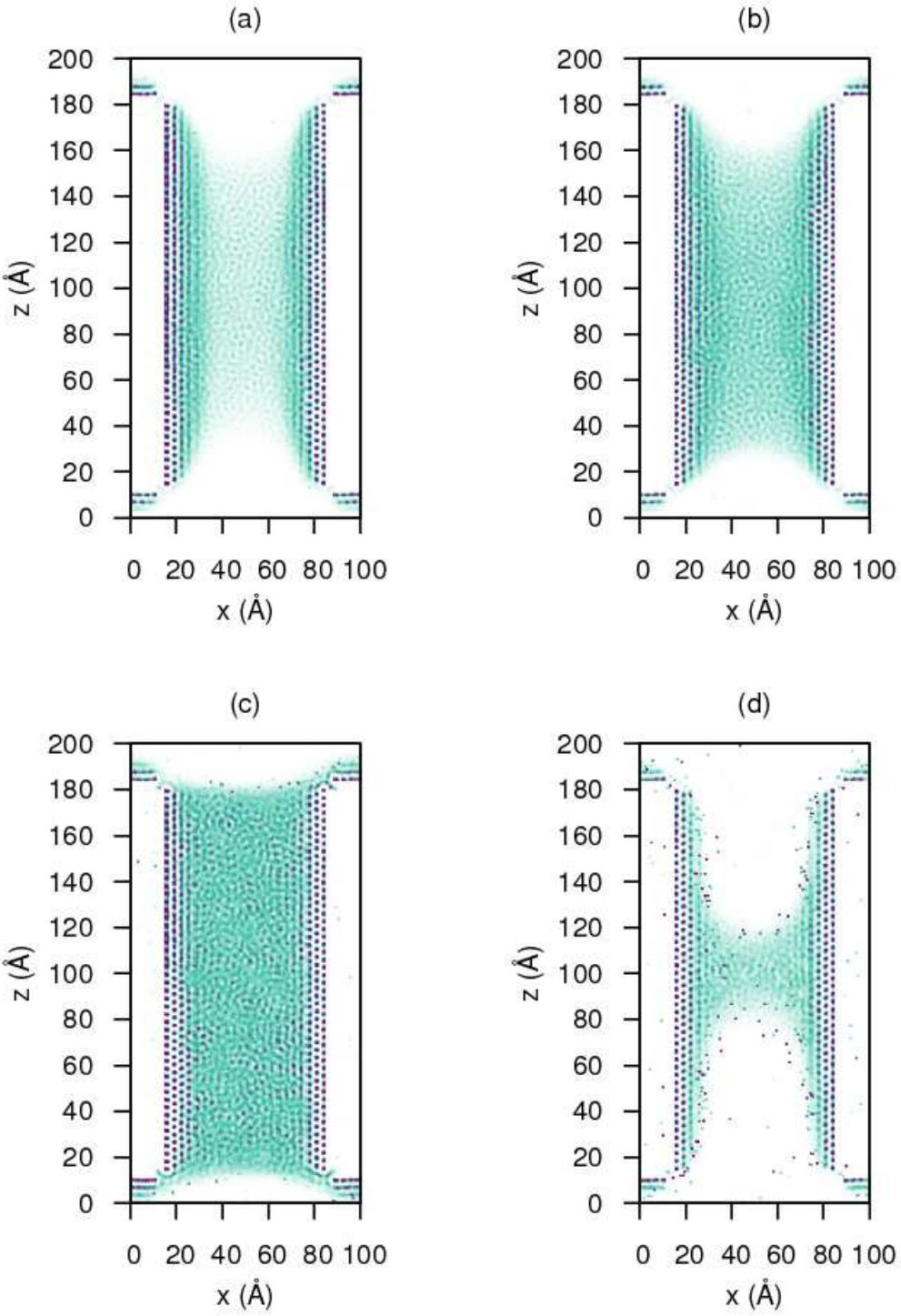

Figure 6. Argon density profile in the open-ended cylindrical pore, during the adsorption phase, at (a) $\Delta\mu$ = -31.4 K (corresponding to N = 12435 atoms in the supercell); (b) $\Delta\mu$ = -29.0 K (N = 15695 atoms); (c) $\Delta\mu$ = -9.6 K (N = 18358 atoms); and during the desorption phase, at (d) $\Delta\mu$ = -59.3 K (N = 7806 atoms). The darker the region, the higher the Argon density.

$\Delta\mu = 17\,K$ (we estimated from our calculated density profiles that the thickness t of the adsorbed film appearing in the expression of the curvatures, $H \propto (r-t)^{-1}$, is roughly about 4 Ar monolayers).

As the pore is being filled, there is no sudden axial condensation as in the case of open pores, so the increase in N with the chemical potential is less abrupt than for the open-ended pore.

At higher values of μ, when the filling of the closed pore is almost complete, the slope of the isotherm decreases, as it happens also for the open-ended pore. In both cases, this portion of the isotherm appears to be linear: for the closed-ended pore, we have calculated a slope of 44.1 ± 1.5 atoms/K; for the open-ended pore, this ratio is approximately twice, because there are two hemispherical meniscii instead of one. During this part of the isotherm, the meniscus remains pinned to the pore circular mouth, while its curvature slowly decreases. In the meantime, a thin film of increasing thickness also appears on the planar portion of the substrate between neighboring pores.

The observed hysteretic behavior for closed-ended pores clearly disagrees with the classical Cohan's model. As discussed in Sec.1, the presence of hysteresis in adsorption experiments in porous materials [13, 14, 16, 21, 42] is usually attributed to a wide pore size distribution, to the presence of surface disorder of the inner walls of the pores, to network effects or, as proposed more recently, to the influence of the porous matrix elasticity during the adsorption/desorption processes.

A recent experimental study [16, 33] of Ar adsorption on an alumina substrate patterned with a regular arrangement of nearly ideal, parallel and unconnected, cylindrical pores with diameters ≈ 10 nm and lengths ≈ 100 μm revealed pronounced hysteresis of the H1-type also in the case of pores closed on one end. The authors attributed it to quenched morphological disorder [14] (likely due to inhomogeneities on a subnanometer scale) on the inner walls of the otherwise very regular pore structure used in these experiments. H1-type hysteresis, indeed, is often attributed to a small degree of disorder [34], whereas most experimental isotherms show instead H2-type loops.

We believe that in our case the hysteresis is caused by the formation of the thin planar liquid film around the pore connecting adjacent pores entrances (see Fig.6c and Fig.7c). During desorption, an energy barrier for tearing such film gives rise to hysteresis. In Ref.[13] it has been suggested that hysteresis in systems of pores closed at one end might be induced by the interplay between the liquid adsorbed on the pore walls and the film adsorbed in the planar region surrounding the pores. This film in the desorption process prevents the concave meniscii from passing through the pore at the expected equilibrium pressure, the emptying of the pore being controlled by the tearing of the film at the edges of the pore itself. Our calculations show that this is what indeed occurs, at least in ideal pores of nanometer sizes.

We are unable to provide at present a numerical estimate for the energy barrier associated with the effect described above, nor its relation with other energy scales in the problem. Such estimate would imply a series of simulations using different pore diameters (we expect that the energy required to tear the film will scale linearly with the length of the pore mouth contour), aimed at relating the hysteresis loop width to the pore diameter. Due to the very long computer times required for such simulations, we must postpone these calculations to a forthcoming work.

A related hysteretic behavior has been recently observed in theoretical calculations of Helium adsorption on substrates nanopatterned with a regular arrangement of parabolic nanocavities [43]. The addition of cavities breaks the planar translational invariance and introduces adsorbing sites of enhanced strength, like

For Peer Review Only

the bottom of the cavity, as well as desorbing sites of reduced strength, like the annular region around the ridge of the cavity. As a result, enhanced hysteretic behavior was observed in the calculated isotherms.

When no film is present in the region surrounding the pore mouths, the resulting isotherms for an ideal pore with one closed end would not show hysteresis. This is the case, for instance, of the molecular dynamics simulations of adsorption/desorption of classical fluids within *isolated* slits with one closed end [10], where no hysteresis is indeed observed.

We mention that hysteresis in closed-end pores was found also in the calculations reported in Ref.[4]. In his work, a small loop in Xenon isotherms on silica-like substrate was found at $T = 85$ K in an array of ideal cylindrical pores $16\,nm$ long and $4\,nm$ wide (i.e. very similar to the ones used in our calculations). Moreover, in a recent paper [29] the adsorption of Ar in graphitic cylindrical single pores was studied at $T = 87.3$ K. Hysteresis has been found in $20.43\,nm$ long closed-ended pores, as long as they are at least $4\,nm$ wide (narrower pores do not show hysteresis); and in $6\,nm$ wide closed-ended pores, as long as they are at least $13.6\,nm$ long. The authors suggested that the pore diameter must be large enough to allow the adsorbate particles in the confined liquid to rearrange, achieving a better packing: in this way, the grand potential well for the metastable states in the desorption branch is deeper, so a lower pressure is needed to make the system jump to the stable state.

At variance with the results presented here, in the simulation accompanying the experimental measurement of Ref.[21], where a geometry very similar to ours is employed (i.e. a periodic array of very regular cylindrical pores, with a comparable aspect ratio), no hysteresis is observed instead in the isotherms for pores with one closed end. We do not have an explanation for such a discrepancy, apart from suggesting that their use of an additional, artificial surface disordering (by randomly moving the substrate atoms) to help the equilibration of their GCMC simulations may actually facilitate the rupture of the thin film, thus narrowing down the hysteretic loop width.

Finally, we remark that in our calculations, due to computational limitations associated with the large number of atoms, we restrict ourselves to nanopores where diameter and length are of the same order of magnitude, whereas in most experimental realizations the pores are usually much longer than wide. This might enhance the contribution to the computed isotherms coming from the pore ends, although pore length effects on hysteresis loops are known to be small [4, 8].

4. Conclusions

We have studied, by using Grand Canonical Monte Carlo simulations, Argon adsorption at T=85 K on a nanostructured Aluminum substrate characterized by a periodic arrangement of cylindrical nanopores either open at both ends or closed at one end. The calculated isotherms exhibit hysteresis loops of type H1 for both kind of substrates. The presence of hysteresis agrees with experimental investigations on porous alumina [16] and silicon [13, 14, 44]. Irreversible adsorption/desorption cycles are observed not only in pores open at both ends, but in pores closed at one end as well, at variance with the classical Cohan model, which predicts no hysteresis for this kind of substrate. While this failure is usually associated to the presence of surface disorder of the inner walls of pores, in our case it is likely related to the presence of a thin film phase on the planar surface between adjacent pores. During desorption, a free energy barrier for tearing such film gives rise to hysteresis. Experimental observations of such effect should employ substrates with geometrically

For Peer Review Only

ordered pores and sharp interfaces, since rounded/irregular pore mouths would probably hinder the observation of the predicted hysteresis loop.

Acknowledgments

We thank Giampaolo Mistura and Benoit Coasne for useful comments and discussions. We acknowledge the support of Padova University through project CPDA077281-07.

References

[1] A. G. Foster, Trans. Faraday. Soc. **28**, 645 (1932).
[2] E. Kierlik, P.A. Monson, M.L. Rosinberg, G.Tarjus, J. Phys. Condens. Matter. **14**, 9295 (2002).
[3] R. Denoyel, R. J. M. Pellenq, Langmuir **18**, 2710 (2002).
[4] L.D. Gelb, Mol. Phys. **100**, 2049 (2002).
[5] M.W.Cole and W.F.Saam, Phys. Rev. Lett. **32**, 985 (1974).
[6] L.H. Cohan, J. Am. Chem. Soc. **60**, 433 (1938).
[7] U. Marini Bettolo Marconi, F. van Swol, Europhys. Lett. **8**, 531 (1989).
[8] A. Papadopoulou, F. van Swol, U. Marini Bettolo Marconi, P. Tarazona, J. Chem. Phys. A **97**, 6942 (1992).
[9] F. Celestini, Phys. Lett. A **228**, 84 (1997).
[10] L. Sarkisov, P. A. Monson, Langmuir **17**, 7600 (2001).
[11] E. A. Ustinov, D. D. Do, J. Chem. Phys. **120**, 9769 (2004).
[12] B. Coasne, F. Di Renzo, A. Galarneau, R.J.M. Pellenq, Langmuir **24**, 7285 (2008).
[13] B. Coasne, A. Grosman, C. Ortega, M. Simon, Phys. Rev. Lett. **88**, 256102 (2002).
[14] D. Wallacher, N. Kunzner, D. Kovalev, N. Knorr, K. Knorr Phys. Rev. Lett. **92**, 195704 (2004).
[15] S.M. Gatica, M.W. Cole, Phys. Rev. E **72**, 041602 (2005).
[16] L. Bruschi, G. Fois, G. Mistura, K. Sklarek, R. Hillebrand, M. Steinhart, U. Gosele, Langmuir **24**, 10936 (2008).
[17] L. Sarkisov, P. A. Monson, Phys. Rev. E **65**, 011202 (2001).
[18] B. Coasne, R. J. M. Pellenq, J. Chem. Phys. **120**, 2913 (2004).
[19] B. Coasne, R. J. M. Pellenq, J. Chem. Phys. **121**, 3767 (2004).
[20] B. Coasne, F. R. Hung, R. J. M. Pellenq, F. R. Siperstein, K. E. Gubbins, Langmuir **22**, 194 (2006).
[21] L. Bruschi, G. Mistura, L. Liu, W. Lee, U. Gosele, B.Coasne, Langmuir **26**, 11894 (2010).
[22] B. Libby and P.A. Monson, Langmuir **20**, 4289 (2004)
[23] J. Puibasset, J. Phys. Chem. B **109**, 480 (2005).
[24] J. Puibasset, J. Phys. Chem. **122**, 134710 (2005); J. Puibasset, Langmuir **25**, 903 (2009); J. Puibasset, J. Phys. Chem. B **109**, 8185 (2005).
[25] J. Puibasset, J. Phys. Chem. B **125**, 074707 (2006).
[26] G. Mason, J. Colloid and Interf. Sci. **88**, 1 (1982).
[27] S. Naumov, R. Valiullin, J. Karger, P.A. Monson, Phys. Rev. E **80**, 031607 (2009).
[28] S. Naumov, A. Khokhlov, R. Valiullin, J. Karger, P.A. Monson, Phys. Rev. E **78**, 060601 (2008).
[29] P. T. M. Nguyen, D. D. Do, D. Nicholson, J. Phys. Chem. C **115**, 4706 (2011).
[30] G. A. Zickler, S. Jahnert, S. S. Funari, G. H. Findenegg, O. C. Paris, J. Appl. Crystallogr. **40**, s522 (2007).
[31] A. Grosman, C. Ortega, Phys. Rev. B **78**, 085433 (2008);
[32] G. Gunther, J. Prass, O. Paris, M. Schoen, Phys. Rev. Lett. **101**, 086104 (2008).
[33] L. Bruschi and G. Mistura, J. Low Temp. Phys. **157**, 206 (2009). A. Grosman, C. Ortega, Langmuir **25(14)**, 8083 (2009).
[34] K. S. W. Sing, D. H. Everett, R. A. Haul, L. Moscou, R. A. Pierotti, J. Rouquerol, T. Siemieniewska, Pure & Appl. Chem. **57**, 603 (1985).
[35] A. Hernando, E. S. Hernandez, R. Mayol, M. Pi, Phys. Rev. B **76**, 115429 (2007).
[36] J. A. Anta, E. Lomba, M. Lombardero, Phys. Rev. E **55**, 2707 (1997).
[37] D. Frenkel, B. Smit, *Understanding Molecular Simulations: From Algorithms to Applications, 2nd ed., Academic Press: London,* (2002).
[38] N. Metropolis, A. W. Rosenbluth, M. N. Rosenbluth, A. H. Teller, E. Teller, J. Chem. Phys. **21**, 1087 (1953).
[39] P.L. Silvestrelli, K. Benyahia, S. Grubišić, F. Ancilotto, F. Toigo, J. Chem. Phys. **130**, 74702 (2009).
[40] C. Schwartz, R. J. Le Roy, Surf. Sci. **166**, L141 (1986).
[41] M. J. Bojan, G. Stan, S. Curtarolo, W. A. Steele and M. W. Cole, Phys. Rev. E **59**, 864 (1999).
[42] F. Casanova, C. E. Chiang, C-P. Li I. V. Roshchin, A. M. Ruminski, M. J. Sailor and I. K. Schuller, Nanotechnology **19**, 315709 (2008).
[43] F. Ancilotto, M. Barranco, E. S. Hernandez, A. Hernando, M. Pi, Phys. Rev. B **79**, 104514 (2009).
[44] A. Grosman, C. Ortega, Langmuir **24**, 3977 (2008).

For Peer Review Only

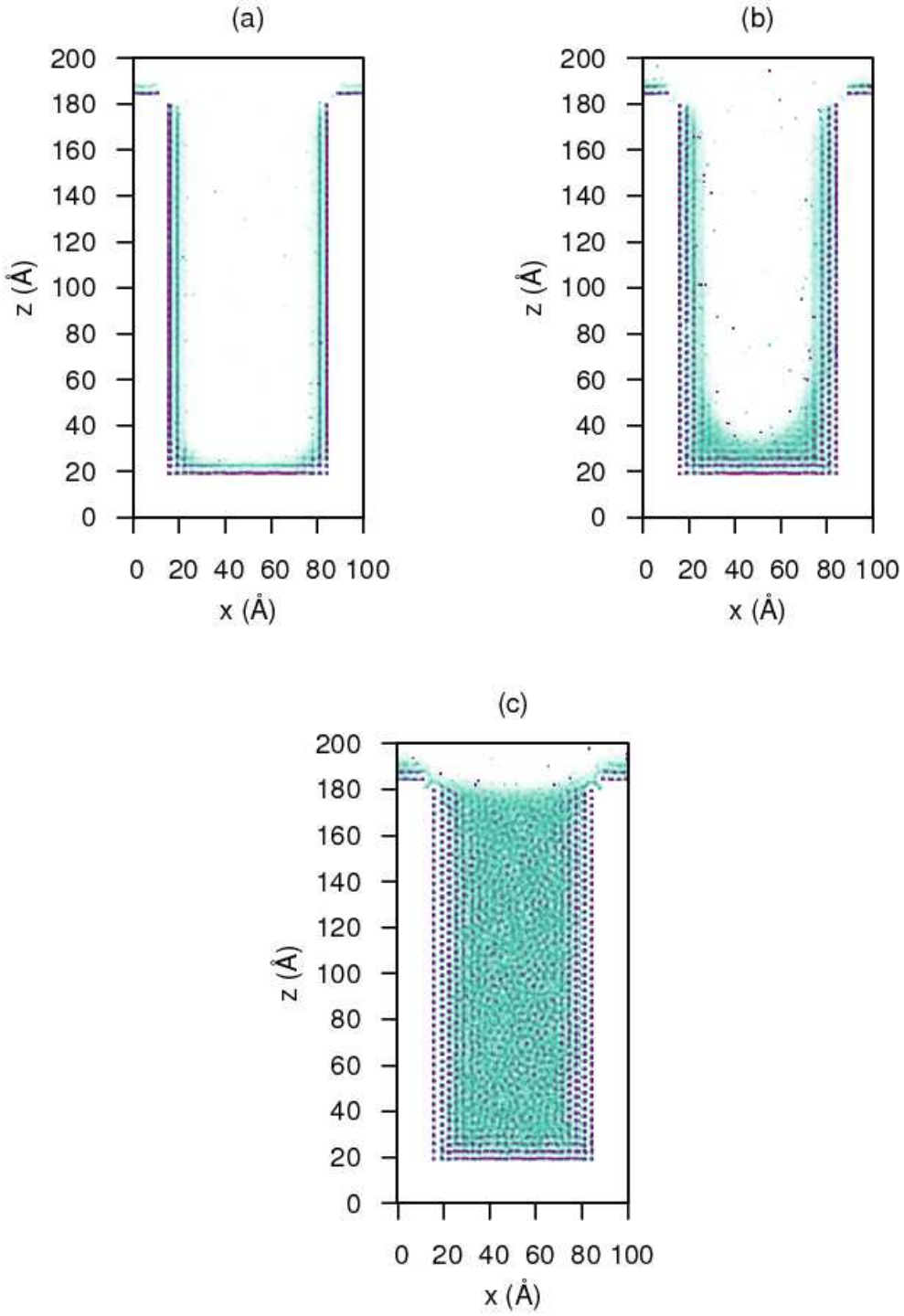

Figure 7. Argon density profile in the closed-ended cylindrical pore, during the adsorption phase, at (a) $\Delta\mu$ = -110.5 K (corresponding to N = 5244 atoms in the supercell); (b) $\Delta\mu$ = -50.6 K (N = 8760 atoms). The darker the region, the higher the Argon density.